Arch Appl Mech (2008) 78: 465–476
DOI 10.1007/s00419-007-0168-3

ORIGINAL

Jiaoxia Lan · Youshi Hong

Micromechanics modeling of strength for nanocrystalline copper

Received: 9 January 2006 / Accepted: 9 February 2007 / Published online: 14 September 2007

Abstract We present a model in this paper for predicting the inverse Hall–Petch phenomenon in nanocrystalline (NC) materials which are assumed to consist of two phases: grain phase of spherical or spheroidal shapes and grain boundary phase. The deformation of the grain phase has an elasto-viscoplastic behavior, which includes dislocation glide mechanism, Coble creep and Nabarro–Herring creep. However the deformation of grain boundary phase is assumed to be the mechanism of grain boundary diffusion. A Hill self-consistent method is used to describe the behavior of nanocrystalline pure copper subjected to uniaxial tension. Finally, the effects of grain size and its distribution, grain shape and strain rate on the yield strength and stress–strain curve of the pure copper are investigated. The obtained results are compared with relevant experimental data in the literature.

Keywords Nanocrystalline materials · Pure copper · Micromechanics · Hall–Petch relation

1 Introduction

In general, NC materials refer to the class of materials whose average grain size is tens of nanometers or smaller than 100 nm. NC materials have attracted much interest from researchers recently due to their superior mechanical properties in comparison with their coarser-grained counterparts. The grain size has a substantial effect on the mechanical properties of metallic materials. Normally, the yield strength is a function of grain size described by Hall–Petch relation, i.e., $\sigma_y = \sigma_0 + Kd^{-0.5}$, where σ_y is the yield stress, σ_0 is the Peierls (friction) stress, K is a constant, and d is the grain size. According to Hall–Petch relation, the yield strength would reach infinity as the grain size tends to zero. This was not an issue in the past, but since NC materials were reported by Birringer et al. [1], many experiments have indicated that Hall–Petch relation did not always hold as the grain size decreased to the nanometer regime. This phenomenon is called inverse Hall–Petch relation.

Many investigations attempted to explain the inverse Hall–Petch relation of NC materials in which two approaches are commonly used. One approach is molecular dynamics (MD) simulation, and the other is rules of mixture. Indeed, MD simulations have made great progress in understanding mechanical properties and deformation behavior of NC materials. But, in this paper only the latter approach will be described in detail. The premise of this approach is that an NC material is considered as a two-phase composite material, including grain and grain boundary phases, since the grain boundaries could occupy relatively significant volume fraction. Thus, the overall yield strength of an NC material can be evaluated as the effective mean of these two phases. For example, Carsley et al. [2] used the mixture rule to obtain the hardness of nickel, iron and copper. Their results showed that a negative slope in the hardness versus $d^{-0.5}$ plot did appear as the grain size

J. Lan (✉) · Y. Hong (✉)
State Key Laboratory of Nonlinear Mechanics (LNM),
Institute of Mechanics, Chinese Academy of Sciences, Beijing 100080, China
E-mail: ljx@lnm.imech.ac.cn
E-mail: hongys@imech.ac.cn

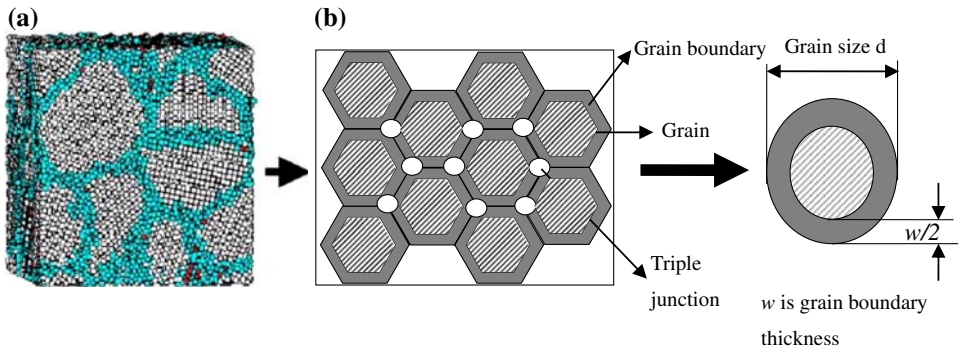

Fig. 1 Two phase model of NC materials

decreased to nanometer regime. Subsequently, Wang et al. [3] also considered a unit cell consisting of crystalline phase and inter-crystalline phase, and adopted different strengths and volume fractions for these regions to estimate the overall flow stress versus $d^{-0.5}$ relation. They also found significant deviation from the traditional Hall–Petch relation. The same unit cell was also made by Kim et al. [4–6] to study the strain-rate sensitivity of the material. They considered that the overall creep rate of the NC metal was the sum of three creep rates of dislocation gliding, lattice diffusion and grain-boundary diffusion plus that of the grain boundary phase. The results suggested that the flow stress increases with decreasing grain size, but in the nanometer regime further decrease in grain size would result in the softening of the material. Another important contribution of this approach was due to Meyers et al. [7,8]. The inner and outer phases are best explained by Ashby's regions of statistically stored dislocations and geometrically necessary ones, respectively. Then using the mixture rule and assuming the thickness of the outer layer to be inverse proportional to the square root of the grain size, we find that the overall stress-strain curve would also follow Hall–Petch relation in the coarse grain region but depart from it as the grain size decreases to nanometer regime.

In this paper, the micromechanics approach is used to investigate inelastic deformation of NC materials. The micro–macro correlation is pursued by volume averaging and by introducing the concepts of stress and strain concentration tensors, which are determined by a self-consistent approach. NC materials are assumed to be composed of two phases: grain phase of spherical and spheroidal shapes as well as grain boundary phase. They have an elasto-viscoplastic deformation behavior by dislocation mechanism. The developed model is applied to pure copper subjected to uniaxial tension. The results are compared with relevant experimental data in the literature.

2 Micromechanics model

The micromechanics model is motivated by recent molecular dynamics simulation of NC materials. Such simulations have been performed by a number of investigators such as, Schiotz et al. [9–11], van Swygenhoven et al. [12,13], Yamakov et al. [14,15], etc. The simulation results suggested that two distinct regions consisting of the grain and the grain boundary are present in NC materials.

The atomistic model from Schiotz et al. [9] is sketched in Fig. 1a, showing the distinct grain and grain boundary phases, and is replaced by a micro-geometry model shown in Fig. 1b. To simplify the analysis, the effect of triple junctions is considered by grain boundary phase in terms of volume fraction. The thickness of grain boundary phase is not negligible in comparison with the grain phase. In addition, perfect bonding between two phases is assumed. The deformation characters of both the grain and the grain boundary phases are elasto-viscoplastic. The grain and grain boundary phases are postulated to be isotropic.

2.1 Grain phase model

It is assumed that the grain shape in an NC material is spherical or spheroidal. When the grains are all spherical in shape, the volume fraction of the grains is $f = \frac{(d-w)^3}{d^3}$, where d is the grain size, and w is the grain boundary

thickness. When the grains are all spheroidal in shape, we define the ellipsoidal domain as:

$$\frac{x_1^2}{a_1^2}+\frac{x_2^2}{a_2^2}+\frac{x_3^2}{a_3^2}\le 1 \tag{1}$$

where $a_i (i = 1, 2, 3)$ is one of the three semi-axes of the ellipsoid. Further, the grain shape is considered to be spheroidal when the condition $a_2 = a_3 = a \neq a_1$ is satisfied. Thus, the volume fraction of grains is $f = \frac{(\beta a - w)(a-w)^2}{\beta a^3}$, where $\beta = \frac{a_1}{a}$, and $a = \frac{d}{2^3\sqrt{\beta}}$.

The constitutive relation of grain is:

$$\dot{\sigma}_{ij}^{\mathrm{g}} = C_{ijkl}^{\mathrm{g}}\left(\dot{\varepsilon}_{kl}^{\mathrm{g}} - \dot{\varepsilon}_{kl}^{\mathrm{vpg}}\right) \tag{2}$$

where $\dot{\sigma}_{ij}^{\mathrm{g}}$ is stress rate of grains, C_{ijkl}^{g} is elastic modulus of grains, $\dot{\varepsilon}_{ij}^{\mathrm{g}}$ is strain rate of grain, and $\dot{\varepsilon}_{ij}^{\mathrm{vpg}}$ is viscoplastic strain rate of grain, which is related to the equivalent viscoplastic strain rate $\dot{\varepsilon}_{\mathrm{eq}}^{\mathrm{vpg}}$ by modified Prandtl–Reuss flow rule:

$$\dot{\varepsilon}_{ij}^{\mathrm{vpg}} = \frac{3}{2}\frac{\dot{\varepsilon}_{\mathrm{eq}}^{\mathrm{vpg}}}{\sigma_{\mathrm{eq}}^{\mathrm{g}}} S_{ij}^{\mathrm{g}} \tag{3}$$

where S_{ij}^{g} and $\sigma_{\mathrm{eq}}^{\mathrm{g}}$ are the deviatoric stress and von Mises equivalent stress of grain, respectively, with:

$$S_{ij}^{\mathrm{g}} = \sigma_{ij}^{\mathrm{g}} - \frac{1}{3}\sigma_{kk}^{\mathrm{g}}\delta_{ij} \tag{4}$$

where δ_{ij} is the Kronecker delta,

$$\delta_{ij} = \begin{cases} 0 & i \neq j \\ 1 & i = j \end{cases} \tag{5}$$

and

$$\sigma_{\mathrm{eq}}^{\mathrm{g}} = \sqrt{\frac{3}{2} S_{ij}^{\mathrm{g}} S_{ij}^{\mathrm{g}}} \tag{6}$$

The strain rate of grain is the sum of three deformation mechanisms, i.e., dislocation glide mechanism, Coble creep mechanism, and lattice diffusion mechanism. Therefore, the equivalent viscoplastic strain rate of grain is:

$$\dot{\varepsilon}_{eq}^{\mathrm{vpg}} = \dot{\varepsilon}^{\mathrm{dis}} + \dot{\varepsilon}^{\mathrm{co}} + \dot{\varepsilon}^{\mathrm{N\text{-}H}} \tag{7}$$

The strain rate of dislocation glide is related to the equivalent stress of grain using the power law [4]:

$$\dot{\varepsilon}^{\mathrm{dis}} = \dot{\varepsilon}^{*}\left(\frac{\sigma_{\mathrm{eq}}^{\mathrm{g}}}{\sigma_0}\right)^{m} Z^{-\frac{m}{2}} \tag{8}$$

The strain rate sensitivity index is defined as:

$$m = \frac{\partial\left(\ln \sum\right)}{\partial\left(\ln \dot{E}\right)} \tag{9}$$

where $\sum$ and $\dot{E}$ are overall equivalent stress and strain rate, respectively, Z is normalized dislocation density, $\dot{\varepsilon}^{*}$ is reference strain rate, and σ_0 is related to the microstructure variables.

The evolution of dislocation density with dislocation glide strain is described by Krausz et al. [16]:

$$\frac{\mathrm{d}Z}{\mathrm{d}\varepsilon^{\mathrm{dis}}} = C + C_1\sqrt{Z} - C_2 Z \tag{10}$$

where C is expressed by:

$$C = M\frac{b}{d}\left(\frac{M\alpha G}{\sigma_0}\right)^2 \tag{11}$$

where M is the Taylor factor which is assumed to be a constant in the present model, b is the Burger vector, G is the shear modulus, α is a material constant, C_1 is a constant accounting for the dislocation storage, and C_2 represents the thermally activated dynamic recovery process given by:

$$C_2 = C_{20}\left(\frac{\dot{\varepsilon}^{\mathrm{dis}}}{\dot{\varepsilon}_0}\right)^{-\frac{1}{n}} \tag{12}$$

where C_{20} and $\dot{\varepsilon}_0$ are material constants, and n is inversely proportional to the temperature and is considered a constant for a given temperature.

The plastic strain rate of grain associated with the Coble creep mechanism [17] is:

$$\dot{\varepsilon}^{\mathrm{co}} = \frac{14\pi\Omega w D_{\mathrm{bd}}\sigma_{\mathrm{eq}}^{\mathrm{g}}}{kTd^3} \tag{13}$$

and that associated with the lattice diffusion mechanism (Nabarro–Herring creep) [18] by:

$$\dot{\varepsilon}^{\mathrm{N\text{-}H}} = \frac{14\pi\Omega D_{\mathrm{ld}}\sigma_{\mathrm{eq}}^{\mathrm{g}}}{kTd^2} \tag{14}$$

where Ω is atomic volume, D_{bd} and D_{ld} are boundary and lattice diffusion coefficients, respectively, k is Boltzman constant, and T is absolute temperature.

2.2 Grain boundary phase model

Since the atoms in grain boundary are arranged relatively loosely, the diffusion mechanism associated with mass transport along the boundaries is considered. The constitutive relation of the grain boundary phase is:

$$\dot{\sigma}_{ij}^{\mathrm{gb}} = C_{ijkl}^{\mathrm{gb}}\left(\dot{\varepsilon}_{kl}^{\mathrm{gb}} - \dot{\varepsilon}_{kl}^{\mathrm{vpgb}}\right) \tag{15}$$

The viscoplastic strain rate of grain boundary phase $\dot{\varepsilon}_{ij}^{\mathrm{vpgb}}$ is related to the equivalent viscoplastic strain rate $\dot{\varepsilon}_{\mathrm{eq}}^{\mathrm{vpgb}}$, according to the modified Prandtl–Reuss flow rule:

$$\dot{\varepsilon}_{ij}^{\mathrm{vpgb}} = \frac{3}{2}\frac{\dot{\varepsilon}_{\mathrm{eq}}^{\mathrm{vpgb}}}{\sigma_{\mathrm{eq}}^{\mathrm{gb}}}S_{ij}^{\mathrm{gb}} \tag{16}$$

where S_{ij}^{gb} and $\sigma_{\mathrm{eq}}^{\mathrm{gb}}$ are deviatoric stress and von Mises equivalent stress of the grain boundary phase, respectively, i.e.,

$$S_{ij}^{\mathrm{gb}} = \sigma_{ij}^{\mathrm{gb}} - \frac{1}{3}\sigma_{kk}^{\mathrm{gb}}\delta_{ij} \tag{17}$$

and

$$\sigma_{\mathrm{eq}}^{\mathrm{gb}} = \sqrt{\frac{3}{2}S_{ij}^{\mathrm{gb}}S_{ij}^{\mathrm{gb}}} \tag{18}$$

The use of Prandtl–Reuss flow rule written by Eqs. (3) and (16) implies that elastic deformation is considered in the following calculation, and that the grain and grain boundary phases are all plastically isotropic.

The equivalent viscoplastic strain rate is equal to the grain boundary diffusion strain rate [5], such that:

$$\dot{\varepsilon}_{\mathrm{eq}}^{\mathrm{vpgb}} = \dot{\varepsilon}^{\mathrm{gb}} = \frac{2\Omega D_{\mathrm{bd}}\sigma_{\mathrm{eq}}^{\mathrm{gb}}}{kTd^2} \tag{19}$$

2.3 Effective nanocrystalline constitutive relation

From a micromechanics point of view, the modeling of heterogeneous materials is based on the averaging operation using the original Eshelby's solution of ellipsoidal inhomogeneity. The self-consistent method is that the interaction among various kinds of inhomogeneities of finite volume concentrations is taken into account by embedding the inhomogeneities in a medium with effective thermomechanical properties. Originally, the self-consistent method has been introduced to describe the elastoplastic behavior of polycrystalline materials with two different approaches: Kroner [19], Budiansky and Wu approach [20] and Hill approach [21]. In the first approach, the elementary problem of inclusion–matrix interaction is solved by taking the difference of plastic strain between the inclusion and surrounding matrix as the Eshelby strain, the constraint power of the matrix remains constant, and therefore overestimates the internal stress. In the second approach where the problem is treated incrementally using the elastoplastic tangent modulus. The constraint power of the matrix depends on the tangent modulus of the matrix, and therefore weakens the internal stress during the plastic deformation. In general, the Hill self-consistent approach shows a better accuracy in describing the behavior of polycrystalline materials and thus can be used for incremental calculations. So Hill's approach is used to derive the constitutive relation of NC materials in the present work. The model is isothermal, neglecting temperature change. The macroscopic constitutive equation is written as:

$$\dot{\sum}_{ij} = C^{\text{eff}}_{ijkl}\left(\dot{E}_{kl} - \dot{E}^{\text{vp}}_{kl}\right) \tag{20}$$

where C^{eff}_{ijkl} is overall elastic modulus, $\dot{E}_{kl}$ is global strain rate, and $\dot{E}^{\text{vp}}_{kl}$ is effective viscoplastic strain rate.

The relations between local strain rate and macroscopic strain rate are given below:

$$\begin{cases} \dot{\varepsilon}^{\text{g}}_{ij} = A^{\text{g}}_{ijkl}\dot{E}_{kl} + a^{\text{g}}_{ij} \\ \dot{\varepsilon}^{\text{gb}}_{ij} = A^{\text{gb}}_{ijkl}\dot{E}_{kl} + a^{\text{gb}}_{ij} \end{cases} \tag{21}$$

where the fourth order concentration tensors A^{g}_{ijkl} and A^{gb}_{ijkl} take into account the heterogeneity of the elastic modulus in the material, and the second order tensors a^{g}_{ij} and a^{gb}_{ij} account for the heterogeneity of inelastic deformation in the material.

It is evident that macroscopic strain and stress rates are, respectively, the volume average of microscopic strain and stress rates. The relations are written as:

$$\dot{E}_{ij} = \frac{1}{v}\int_v \dot{\varepsilon}_{ij}dv = \left\langle \dot{\varepsilon}_{ij} \right\rangle_v \tag{22}$$

and

$$\dot{\Sigma}_{ij} = \frac{1}{v}\int_v \dot{\sigma}_{ij}dv = \left\langle \dot{\sigma}_{ij} \right\rangle_v \tag{23}$$

Equations (22) and (23) are the definitions of general case, and the average strain rate $\dot{E}_{ij}$ and the average stress rate $\dot{\Sigma}_{ij}$ are consistent in the following analysis.

The relations between microscopic and macroscopic strain and stress rate are given below:

$$\dot{\varepsilon}_{ij} = A_{ijkl}\dot{E}_{kl} + a_{ij} \tag{24}$$

and

$$\dot{\sigma}_{ij} = B_{ijkl}\dot{\sum}_{kl} + b_{ij} \tag{25}$$

where A_{ijkl} and B_{ijkl}, are respectively the fourth- order strain and stress concentration tensors while a_{ij} and b_{ij} are the corresponding second order tensors.

Substitution equations (24) and (25) into equations (22) and (23) will result in the following:

$$\left\langle A_{ijkl} \right\rangle_v = \left\langle B_{ijkl} \right\rangle_v = I_{ijkl} \tag{26}$$

and

$$\langle a_{ij} \rangle_v = \langle b_{ij} \rangle_v = 0 \tag{27}$$

where

$$I_{ijkl} = \frac{1}{2}\left(\delta_{ik}\delta_{jl} + \delta_{il}\delta_{jk}\right) \tag{28}$$

Substituting equations (24) and (25) into Eqs. (2) and (15), and comparing with Eq. (20), then using Eqs. (26) and (27), we find

$$C^{\text{eff}}_{ijkl} = \langle C_{ijmn} A_{mnkl} \rangle_v \tag{29}$$

$$\dot{E}^{\text{vp}}_{ij} = \left(C^{\text{eff}}_{ijkl}\right)^{-1} \langle C_{klmn}\dot{\varepsilon}^{\text{vp}}_{mn} - C_{klmn} a_{mn} \rangle_v \tag{30}$$

The volumes of two phases are denoted by v^{g}, v^{gb}, respectively. So we obtain:

$$C^{\text{eff}}_{ijkl} = (1-f) C^{\text{gb}}_{ijmn} A^{\text{gb}}_{mnkl} + f C^{\text{g}}_{ijmn} A^{\text{g}}_{mnkl} \tag{31}$$

$$\dot{E}^{\text{vp}}_{ij} = \left(C^{\text{eff}}_{ijmn}\right)^{-1} \left[f C^{\text{g}}_{mnkl}\left(\dot{\varepsilon}^{\text{vpg}}_{kl} - a^{\text{g}}_{kl}\right) + (1-f) C^{\text{gb}}_{mnkl}\left(\dot{\varepsilon}^{\text{vpgb}}_{kl} - a^{\text{gb}}_{kl}\right)\right] \tag{32}$$

The expressions [22] of the fourth-order tensors and the second-order tensors are expressed as follows, respectively:

$$A^{\text{g}}_{ijkl} = \left[I_{ijkl} + S_{ijmn}\left(C^{\text{eff}}\right)^{-1}_{mnpq}\left(C^{\text{g}}_{pqkl} - C^{\text{eff}}_{pqkl}\right)\right]^{-1} \tag{33}$$

$$A^{\text{gb}}_{ijkl} = \left[I_{ijkl} + S_{ijmn}\left(C^{\text{eff}}\right)^{-1}_{mnpq}\left(C^{\text{gb}}_{pqkl} - C^{\text{eff}}_{pqkl}\right)\right]^{-1} \tag{34}$$

$$a^{\text{g}}_{ij} = A^{\text{g}}_{ijkl} S_{klmn}\left(C^{\text{eff}}\right)^{-1}_{mnpq}\left(C^{\text{g}}_{pqrs}\dot{\varepsilon}^{\text{vpg}}_{rs} - C^{\text{eff}}_{pqrs}\dot{E}^{\text{vp}}_{rs}\right) \tag{35}$$

$$a^{\text{gb}}_{ij} = -A^{\text{gb}}_{ijkl} S_{klmn}\dot{E}^{vp}_{mn} \tag{36}$$

where S_{ijkl} is Eshelby's tensor [see Appendix].

3 Results and discussion

We now apply the developed model to evaluate the stress-strain relation and yield strength of pure copper subjected to uniaxial tension as the grain size decreases from coarse grain to nanometer regime. The values of shear modulus and Poisson's ratio of grain and grain boundary phases used in the calculation are $\mu^{\text{g}} = 42.1\text{GPa}$, $\nu^{\text{g}} = 0.3$ and $\mu^{\text{gb}} = 25.26\text{GPa}$, $\nu^{\text{gb}} = 0.33$, respectively. The other parametric values [4] are $\dot{\varepsilon}^* = 0.005\text{s}^{-1}$, $\sigma_0 = 160\,\text{MPa}$, $M = 3.06$, $\alpha = 0.33$, $G = 42.1\,\text{GPa}$, $b = 25.6\,\text{nm}$, $C_1 = 52.86$, $C_{20} = 40.5$, $n = 21.25$, $\dot{\varepsilon}_0 = 0.001\,\text{s}^{-1}$, $\Omega = 1.18 \times 10^{-29}\,\text{m}^3$, $k = 1.38 \times 10^{-23}\,\text{Pa}\,\text{m}^3$, $T = 300\,\text{K}$, $D_{\text{bd}} = 2.6 \times 10^{-20}\text{m}^2\,\text{s}^{-1}$, $D_{\text{ld}} = 1.512 \times 10^{-40}\text{m}^2\,\text{s}^{-1}$.

A set of equations (2), (7), (8)–(14) were used to calculate the grain phase deformation behavior, and equations (15)–(19) were used for grain boundary phase. Finally, equations (20)–(21), and (31)–(36) were applied to investigate the overall deformation behavior. Implicit iteration algorithm was employed in this calculation. Then, the curves of stress–strain at different grain sizes under different strain rates, and of yield strength versus grain size are obtained. The predicted behavior was compared with the experimental data in the literature.

3.1 Spherical grains

In this section, we discuss the effect of spherical grains on the stress–strain relations and yield strength for pure copper subjected to uniaxial tension.

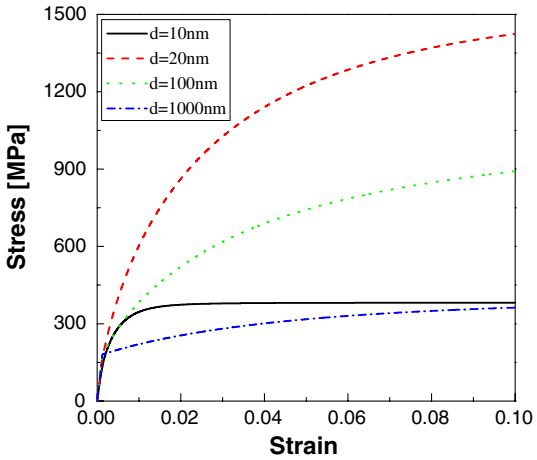

Fig. 2 Stress–strain relations for Cu of different grain sizes with strain rate of $1 \times 10^{-3}\,\mathrm{s}^{-1}$

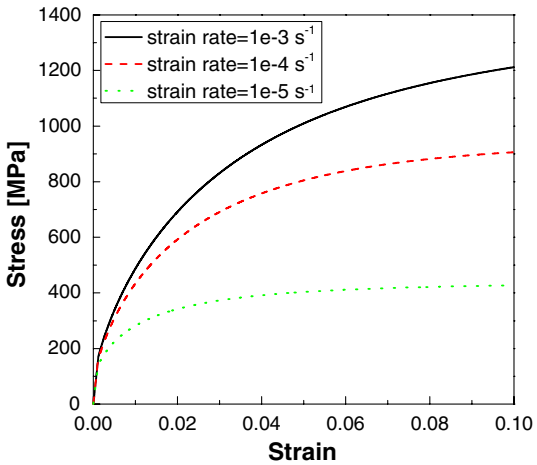

Fig. 3 Stress–strain relations for Cu under different strain rates with average grain size of 49 nm

3.1.1 Without considering the distribution of grain size

The stress–strain curves of different grain sizes under different strain rates are plotted in Fig. 2. The results indicate that the flow stress of coarse grain Cu (1,000 nm) is the lowest, and it increases with the decrease in grain size. However, as the grain size approaches to the critical value, further decrease in grain size leads to the decrease in flow stress.

The stress–strain relations under different strain rates are plotted in Figs. 3, 4 and 5. It is shown that the flow stress increases with the increase in strain rate, but the amplitude variation is sensitive to grain size.

Figure 6 shows the stress–strain curves of different grain sizes under the strain rate of $1 \times 10^{-3}\,\mathrm{s}^{-1}$, and the colored dots in the figure are the experimental data in the literature [23,24]. Our calculated results are in good agreement with experimental data when the strain is less than 2%.

The yield strength versus inverse square grain size curves are plotted in Fig. 7 for the strain rate of $1\times10^{-3}s^{-1}$. The solid line is the result predicted by the present model while the dots correspond to the experimental data [23,25,26]. It is shown that the yield stress increases with decreasing grain size, when the grain size is larger, but as the grain size arrives at critical scale, the yield stress starts to decrease with decreasing grain size when the grain size is smaller. The predicted yield stress of NC materials is in agreement with the experimental data. This phenomenon is the so-called inverse Hall–Petch relation that has been reported in a number of investigations [1–7].

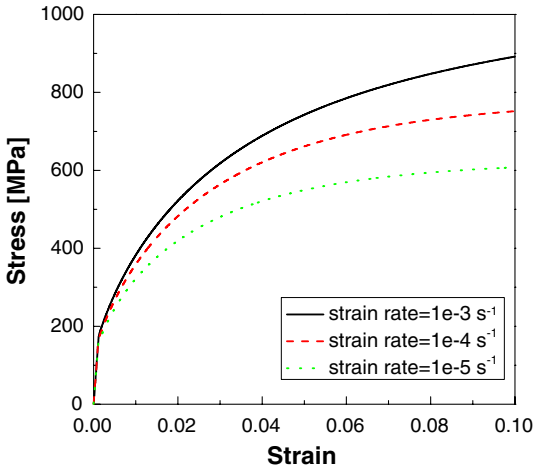

Fig. 4 Stress–strain relations for Cu under different strain rates with average grain size of 100 nm

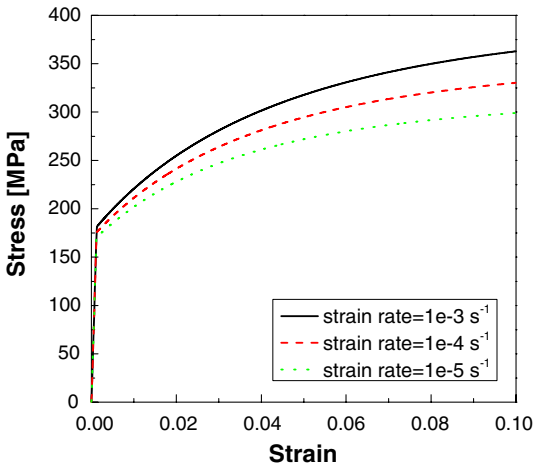

Fig. 5 Stress–strain relations for Cu under different strain rates with average grain size of 1,000 nm

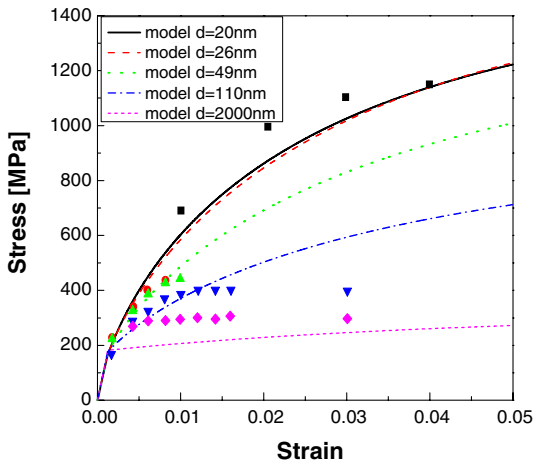

Fig. 6 Comparison of stress–strain relations predicted by present model with experimental data in literature for strain rate of 1×10^{-3} s^{-1}

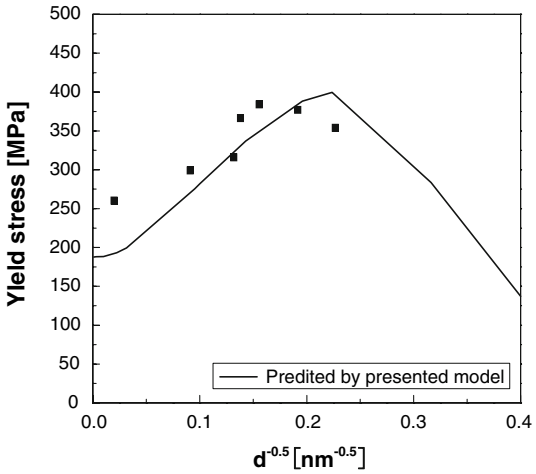

Fig. 7 Comparison of yield strength versus grain size relations predicted by present model with experimental data for strain rate of 1×10^{-3} s^{-1}

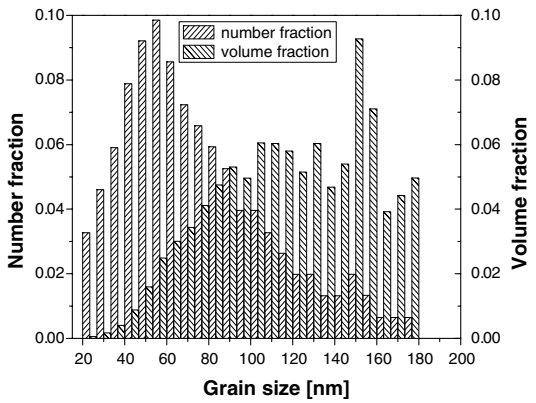

Fig. 8 Statistical distribution of grain size for copper [27]. About 300 grains were measured for the sample

3.1.2 Considering the distribution of grain size

Many experimental results demonstrated that there are great difference in flow stress or hardness although the average grain size was the same. In order to interpret the phenomenon, we investigate the influence of distribution of grain size. A given distribution of grain size consists of several size ranges, each range being of its volume fraction, i.e., the contribution of different grain sizes is in inequality, then the mixture rule will be applied for this case.

The statistical distribution of grain size for pure Cu is reproduced in Fig. 8, with the average grain size of 75 nm. Figure 9 shows the effect of distribution of grain sizes on stress–strain relations. It is seen that, with considering the distribution of grain size, the flow stress decreases in comparison with the uniform distribution of grain size.

3.2 Spheroidal grains

In this section, we investigate the influence of spheroidal grains on stress–strain curves for pure copper subjected to uniaxial tension with considering distribution of grain size. The direction of uniaxial load is correspondent to a_1 axis (i.e., x direction).

The effect of β (as defined in 2.1) on stress is shown in Figs. 10 and 11. The results indicate that the flow stress increases with the increase in parameter β. Such an increase is substantial as β is larger than one, but it diminishes as β is less than one.

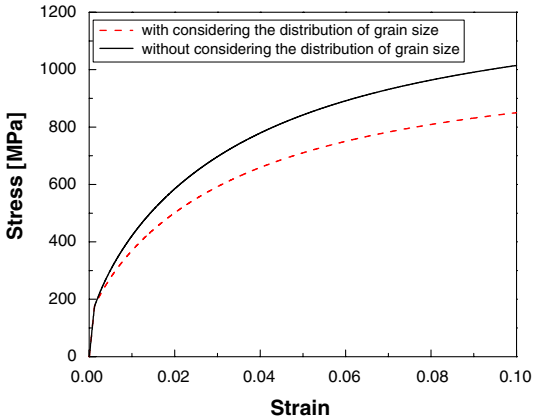

Fig. 9 Stress–strain relations of pure Cu with and without considering distribution of grain size with d of 75 nm and strain rate of 1×10^{-3} s^{-1}

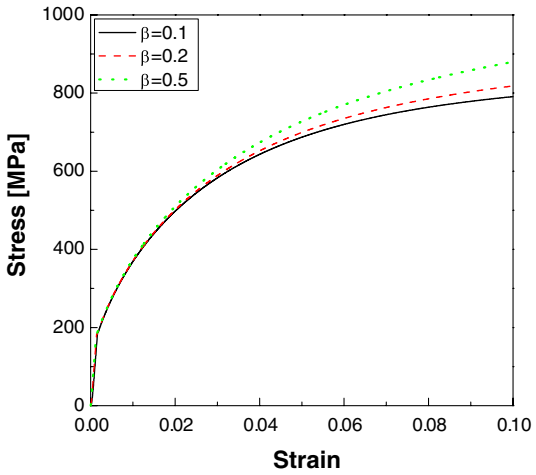

Fig. 10 Stress–strain relations for pure Cu for different parameter β values less than one with d of 75 nm and strain rate of 1×10^{-3} s^{-1}

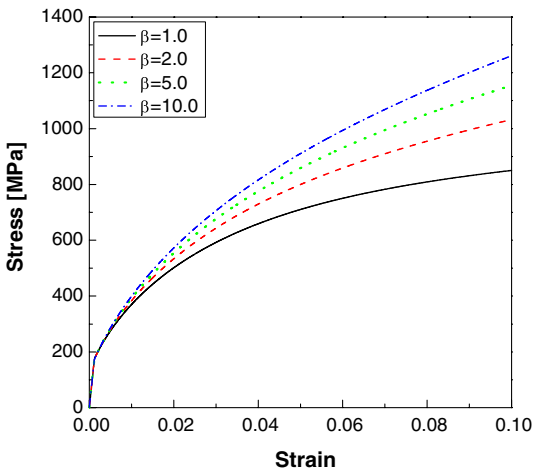

Fig. 11 Stress–strain relations for pure Cu for different parameter β values larger than one with d of 75 nm and strain rate of 1×10^{-3} s^{-1}

4 Summary

The paper is the extension of existing two-phase models incorporating a third element, the triple junctions. The elastic deformation is included and a self-consistent approach has been adopted. The paper addresses the mechanical response of nanocrystalline materials, as exemplified by copper, in terms of an elastic-viscoplastic model in which the grain phase of spherical (or spheroidal) shape and grain boundary phase are separated phases with distinct constitutive behavior.

In this paper, the micro–macro correlation is realized by volume averaging and by introducing the concepts of stress and strain concentration tensors which are determined by self-consistent approach. A micromechanics method was presented and applied to pure copper subjected to uniaxial tension so as to analyze the dependence of grain sizes and strain rates on yield strength and stress–strain curve, respectively. In addition, the influence of grain size distribution and grain shape on stress–strain curve was also investigated. The following results are obtained:

(1) Flow stress increases with a decrease in grain size before it approaches to the critical value.
(2) Flow stress increases with an increase in strain rate, but the amplitude variation is sensitive to grain size.
(3) The stress–strain relations of different grain sizes given by the developed model agree well with experimental data.
(4) The breakdown of Hall–Petch relation is reproduced. During the transition from the Hall–Petch relation to one with a negative slope, both grain phase and grain boundary phase contribute competitively to the overall plastic deformation of the nanocrystalline materials.
(5) Considering the distribution of grain size, one finds that flow stress decreases in comparison with the uniform distribution of grain size.
(6) Flow stress increases with an increase in parameter β.

Moreover, more experiments and simulations are needed to verify the model for different materials.

Acknowledgments This paper was supported by the National Nature Science Foundation of China (10472117), and the Chinese Academy of Sciences.

Appendix

Eshelby (1957) proved that the Eshelby's tensor does not depend on the location of the point in an inclusion. Explicitly, the Eshelby's tensor for a *spheroidal* grain is [28,29]:

$$S_{ijkl} = \frac{1}{4\left(1-\nu^{\mathrm{gb}}\right)}\left[S^{(1)}_{IK}\delta_{ij}\delta_{kl} + S^{(2)}_{IJ}\left(\delta_{ik}\delta_{jl}+\delta_{il}\delta_{jk}\right)\right] \tag{A.1}$$

In which the following summation convention has been used: repeated lower case indices are summed over from one to three; upper case indices take on the same numbers as the corresponding lower case ones but are not summed. The components of the Eshelby's tensor for a *spheroidal* inclusion can be explicitly described as:

$$S^{(1)}_{11} = \left[4\nu^{\mathrm{gb}} + \frac{2}{\beta^2-1}\right]g(\beta) + 4\nu^{\mathrm{gb}} + \frac{4}{3\left(\beta^2-1\right)} \tag{A.2}$$

$$S^{(1)}_{12} = S^{(1)}_{13} = \left[4\nu^{\mathrm{gb}} - \frac{2\beta^2+1}{\beta^2-1}\right]g(\beta) + 4\nu^{\mathrm{gb}} - \frac{2\beta^2}{\beta^2-1} \tag{A.3}$$

$$S^{(1)}_{21} = S^{(1)}_{31} = \left[-2\nu^{\mathrm{gb}} - \frac{2\beta^2+1}{\beta^2-1}\right]g(\beta) - \frac{2\beta^2}{\beta^2-1} \tag{A.4}$$

$$S^{(1)}_{22} = S^{(1)}_{23} = S^{(1)}_{32} = S^{(1)}_{33} = \left[-2\nu^{\mathrm{gb}} + \frac{4\beta^2-1}{4\left(\beta^2-1\right)}\right]g(\beta) + \frac{\beta^2}{2\left(\beta^2-1\right)} \tag{A.5}$$

$$S^{(2)}_{11} = \left[-4\nu^{\mathrm{gb}} + \frac{4\beta^2-2}{\beta^2-1}\right]g(\beta) - 4\nu^{\mathrm{gb}} + \frac{12\beta^2-8}{3\left(\beta^2-1\right)} \tag{A.6}$$

$$S^{(2)}_{12} = S^{(2)}_{13} = S^{(2)}_{21} = S^{(2)}_{31} = \left[-\nu^{\mathrm{gb}} - \frac{\beta^2+2}{\beta^2-1}\right]g(\beta) - 2\nu^{\mathrm{gb}} - \frac{2}{\beta^2-1} \tag{A.7}$$

$$S^{(2)}_{22} = S^{(2)}_{23} = S^{(2)}_{32} = S^{(2)}_{33} = \left[2\nu^{\mathrm{gb}} - \frac{4\beta^2-7}{4\left(\beta^2-1\right)}\right]g(\beta) + \frac{\beta^2}{2\left(\beta^2-1\right)} \tag{A.8}$$

where $\beta = \frac{a_1}{a}$, and $g(\beta)$ is given by:

$$g(\beta) = \begin{cases} \dfrac{\beta}{\left(\beta^2-1\right)^{\frac{3}{2}}}\left[\cosh^{-1}\beta - \beta\left(\beta^2-1\right)^{\frac{1}{2}}\right] & \text{for} \quad \beta > 1 \\ \dfrac{\beta}{\left(1-\beta^2\right)^{\frac{3}{2}}}\left[\beta\left(\beta^2-1\right)^{\frac{1}{2}} - \cos^{-1}\beta\right] & \text{for} \quad \beta < 1 \end{cases} \tag{A.9}$$

Specially, for the special case of a spherical grain ($\beta = 1$), the Eshelby's tensor reduces to:

$$S_{ijkl} = \frac{1}{15\left(1-\nu^{\mathrm{gb}}\right)}\left[\left(5\nu^{\mathrm{gb}}-1\right)\delta_{ij}\delta_{kl} + \left(4-5\nu^{\mathrm{gb}}\right)\left(\delta_{ik}\delta_{jl}+\delta_{il}\delta_{jk}\right)\right] \tag{A.10}$$

References

1. Birringer, R., Gleiter, H., Klein, H.-P., Marquardt, P.: Nanocrystalline materials: an approach to a novel solid structure with gas-like disorder. Phys. Lett. **102**, 365–369 (1984)
2. Carsley, J.E., Ning, J., Milligan, W.W., Hackney, S.A., Aifantis, E.C.: A simple mixture based model for the grain size dependence of strength in nanophase metals. Nanostruct. Mater. **5**, 441–448 (1995)
3. Wang, N., Wang, Z., Aust, K.T., Erb, U.: Effect of grainsize on mechanical properties of nanocrystalline materials. Acta Metall. Mater. **43**, 519–528 (1995)
4. Kim, H.S., Estrin, Y., Bush, M.: Plastic deformation behaviors of fine grained materials. Acta Mater. **48**, 493–504 (2000)
5. Kim, H.S., Estrin, Y., Bush, M.: Constitutive modeling of strength and plasticity of nanocrystalline metallic materials. Mater. Sci. Eng. A **316**, 195–199 (2001)
6. Kim, H.S., Estrin, Y.: Phase mixture modeling of strain rate dependent mechanical behavior of nanostructured materials. Acta Mater. **53**, 765–772 (2005)
7. Benson, D.J., Fu, H.H., Meyers, M.A.: On the effect of grain size on yield stress: extension into nanocrystalline domain. Mater. Sci. Eng. A 319–321, 854–861 (2001)
8. Fu, H., Benson, D.J., Meyers, M.A.: Analytical and computational description of effect of grain size on yield stress of metals. Acta Mater. **49**, 2567–2582 (2001)
9. Schiotz, J., Di Tolla, F.D., Jacobsen, K.W.: Softening of nanocrystalline metals at very small grain sizes. Nature **39**, 561–563 (1998)
10. Schiotz, J., Jacobsen, K.W.: A maximum in the strength of nanocrystalline copper. Science **301**, 1357–1359 (2003)
11. Schiotz, J., Vegge, T., Di Tolla, F.D., Jacobsen, K.W.: Atomic-scale simulations of the mechanical deformation of nanocrystalline metals. Phys. Rev. B **60**, 11971–11983 (1999)
12. Van Swygenhoven, H., Spaczer, M., Caro, A.: Microscopic description of plasticity in computer generated metallic nanophase samples: a comparison between Cu and Ni. Acta Mater. **47**, 3117–3126 (1999)
13. Derlet, P.M., Swygenhoven, H.V.: Length scale effects in the simulation of deformation properties of nanocrystalline metals. Scripta Mater. **47**, 719–724 (2002)
14. Yamakov, V., Wolf, D., Phillpot, S.R., Gleiter, H.: Grain-boundary diffusion creep in nanocrystalline palladium by molecular dynamics simulation. Acta Mater. **50**, 61–73 (2002)
15. Yamakov, V., Wolf, D., Salazar, M., Phillpot, S.R., Geiter, H.: Length-scale effects in the nucleation of extended dislocations in nanocrystalline Al by molecular dynamics simulation. Acta Mater. **49**, 2713–2722 (2001)
16. Krausz, A.S., Krausz, K.: Unified Constitutive Laws of Plastic Deformation. Academic, San Diego (1996)
17. Coble, R.L.: A model for boundary diffusion controlled creep in polycrystalline materials. J. Appl. Phys. **34**, 1679–1682 (1963)
18. Herring, C.: Diffusional viscosity of a polycrystalline solid. J. Appl. Phys. **21**, 437–445 (1950)
19. Kroner, E.: Zur plastischen verformung des Vielkristalls. Acta Metall. **9**, 155 (1961)
20. Budiansky, B., Wu, T.T.: Theory prediction of plastic strains of polycrystals. In: Proc. 4th. U. S. Nat. Congr. Appl. Mech. 1175 (1962)
21. Hill, R.: Continuum micro-mechanics of elastoplastic polycrystals. J. Mech. Phys. Solids **13**, 89–101 (1965)
22. Cherkaoui, M., Sun, Q.P., Song, G.P.: Micromechanics modelling of composite with ductile matrix and shape memory alloy reinforcement. Int. J. Solid Struct. **37**, 1577–1594 (2000)
23. Sanders, P.G., Eastman, J.A., Weertman, J.R.: In: Suryanarayana, C., Singh, J., Froes, F.H. (Eds.) Processing and Properties of Nanocrystalline Materials. TMS, Warrendale, pp. 397–405 (1996)
24. Youngdahl, C.J., Sanders, P.G., Eastman, J.A., Weertman, J.R.: Compressive yield strengths of nanocrystalline Cu and Pd. Scripta Mater. **37**, 809–813 (1997)
25. Sanders, P.G., Eastman, J.A., Weertman, J.R.: Elastic and tensile behaviour of nanocrystalline copper and palladium. Acta Mater. **45**, 4019–4025 (1997)
26. Suryanarayanan, R., Frey, C.A., Sastry, S.M.L., Waller, B.E., Bates, S.E., Buhro, W.E.: Deformation, recovery, and recrystallization behavior of nanocrystalline copper produced by solution phase synthesis. J. Mater. Res. **11**, 439–443 (1996)
27. Zhao, Y.H., Liao, X.Z., Zhu, Y.T., Horita, Z., Langdon, T.G.: Influence of stacking fault energy on nanostructure formation under high pressure torsion. Mater. Sci. Eng. A 410–411, 188–193 (2005)
28. Mura, T.: Micromechanics of Defects in Solids. Martinus Nijhoff Publishers, The Hague (1982)
29. Ju, J.W., Sun, L.Z.: Effective elastoplastic behavior of metal matrix composites containing randomly located aligned spheroidal inhomogeneties. Int. J. Solid Struct. **38**, 183–201 (2001)